Structure of the Redox Sensor Domain of *Azotobacter vinelandii* NifL at Atomic Resolution: Signaling, Dimerization, and Mechanism[†,‡]

Jason Key,[§,||] Marco Hefti,[⊥] Erin B. Purcell,[§] and Keith Moffat*[,§,#,△]

Department of Biochemistry and Molecular Biology, Consortium for Advanced Radiation Sources, and Institute for Biophysical Dynamics, University of Chicago, Chicago, Illinois 60637, and Laboratory of Biochemistry, Wageningen University, Wageningen, The Netherlands

Received September 30, 2006; Revised Manuscript Received January 23, 2007

ABSTRACT: NifL is a multidomain sensor protein responsible for the transcriptional regulation of genes involved in response to changes in cellular redox state and ADP concentration. Cellular redox is monitored by the N-terminal PAS domain of NifL which contains an FAD cofactor. Flavin-based PAS domains of this type have also been referred to as LOV domains. To explore the mechanism of signal recognition and transduction in NifL, we determined the crystal structure of the FAD-bound PAS domain of NifL from *Azotobacter vinelandii* to 1.04 Å resolution. The structure reveals a novel cavity within the PAS domain which contains two water molecules directly coordinated to the FAD. This cavity is connected to solvent by multiple access channels which may facilitate the oxidation of the FAD by molecular oxygen and the release of hydrogen peroxide. The structure contains a dimer of the NifL PAS domain that is structurally very similar to those described in other crystal structures of PAS domains and identifies a conserved dimerization motif. An N-terminal amphipathic helix constitutes part of the dimerization interface, and similar N-terminal helices are identified in other PAS domain proteins. The structure suggests a model for redox-mediated signaling in which a conformational change is initiated by redox-dependent changes in protonation at the N5 atom of FAD that lead to reorganization of hydrogen bonds within the flavin binding pocket. A structural signal is subsequently transmitted to the β-sheet interface between the monomers of the PAS domain.

The ability to fix nitrogen allows diazotrophs to thrive in environments of severe nitrogen deprivation. These organisms are able to colonize otherwise inaccessible environments, but this benefit comes at a cost. Nitrogen fixation demands large amounts of energy (*2*), and due to the oxygen sensitivity of the enzyme nitrogenase, organisms must protect this essential protein from irreversible inhibition by oxygen. To cope with these requirements, nitrogen-fixing organisms regulate the expression of nitrogen fixation genes in response to the concentration of oxygen and the availability of energy. In the free living γ-proteobacterium *Azotobacter vinelandii* the oxygen sensitivity of nitrogenase must be reconciled with a strictly aerobic metabolism. These bacteria have evolved a number of protection mechanisms to ensure that nitrogenase is not damaged by oxygen (*2*−*5*). A major component of this regulation mechanism is the NifL−NifA regulatory system, in which the flavoprotein NifL regulates the activity of the transcriptional activator NifA in response to oxygen concentration and cellular redox state (*6*). In contrast to heme-based oxygen sensors which detect oxygen directly (*7*), NifL detects oxygen through changes in the redox state of its FAD prosthetic group.

A. vinelandii NifL (*Av*NifL) is a modular, tetrameric protein (*8*) in which each monomer is composed of three linked domains: two N-terminal Per-ARNT-Sim (PAS) domains are connected by a Q-linker region (*9*) to a C-terminal domain whose sequence is homologous to the histidine kinases of bacterial two-component signaling systems. PAS domains form a large and diverse family of structurally homologous domains found in all kingdoms of life (*10*). The roles of PAS domains are quite diverse. Some bind prosthetic groups such as heme, FMN, or FAD, though others do not. As a class they exhibit low sequence homology but high tertiary structural homology (*11*). The N-terminal, FAD-containing, PAS domain of *A. vinelandii* NifL (referred to here as *Av*NifLF) is responsible for the redox-mediated regulation of the transcriptional activator NifA, a member of the family of sigma factor 54 (σ^{54}) dependent transcriptional activators (*12*, *13*).

The C-terminal kinase-like domain of NifL does not exhibit kinase activity (*9*) but is required for binding of NifL to the activator NifA. Although there is significant sequence

[†] This work was supported by NIH Grant GM036452 to K.M. BioCARS is supported by NIH Grant RR07707 to K.M.; the Advanced Photon Source is supported by the Department of Energy.

[‡] The structure and structure factors have been deposited in the Protein Data Bank under PDB ID 2GJ3.

* To whom correspondence should be addressed at the Department of Biochemistry and Molecular Biology, University of Chicago. E-mail: moffat@cars.uchicago.edu. Phone: 773-702-2116. Fax: 773-702-0439.

[§] Department of Biochemistry and Molecular Biology, University of Chicago.

[||] Current address: Department of Biophysics, Vrije Universiteit, Amsterdam, The Netherlands.

[⊥] Laboratory of Biochemistry, Wageningen University.

[#] Consortium for Advanced Radiation Sources (CARS), University of Chicago.

[△] Institute for Biophysical Dynamics, University of Chicago.

10.1021/bi0620407 CCC: $37.00
Published on Web 02/24/2007

homology between kinase effector domains of bacterial two-component systems and the C-terminal domain of NifL, signal transduction between NifL and NifA is transmitted directly through protein−protein interactions and not via phosphorylation (*8*, *14*, *15*). In the absence of oxygen, the FAD of NifL is reduced and NifA is free to activate σ^{54}-dependent gene transcription, including the *nif* regulon which encodes the majority of nitrogen fixation genes. Upon oxidation of the FAD, NifL acts as an antiactivator and binds to NifA to prevent activation of nitrogenase expression. The NifL holoprotein has a redox potential of −226 mV at pH 8 and can be reduced by a variety of cellular electron donors (*16*). The physiological electron donor to *Av*NifL in *A. vinelandii* is not known. Oxygen is most likely to be the physiological oxidant; *Av*NifL is rapidly oxidized upon exposure to air, yielding hydrogen peroxide as a product (*17*). Studies of the related FAD-based PAS oxygen sensor, *Escherichia coli* aer (AER), revealed a number of residues important for proper binding of the FAD group and in vivo signaling (*18*). Nevertheless, the molecular mechanism of redox sensing has not been elucidated.

Related FMN-based photoreceptor PAS domains, often referred to as *l*ight *o*xygen *v*oltage (LOV) domains,[1] have been the subject of numerous studies that reveal much about their signaling mechanism (*1*). The high degree of sequence homology between redox and photoreceptor LOV domains suggests common mechanistic elements. LOV domains were first identified as the primary sensor for phototropism in higher plants and sexual development in green algae (*19*, *20*). These domains were later demonstrated to form a light-dependent covalent cysteinyl adduct between the C4a atom of FMN and a nearby conserved cysteine side chain (*21*, *22*). Harper and colleagues subsequently identified light-dependent conformational changes in a C-terminal helical extension of the core PAS domain which packs directly opposite the chromophore on the external surface of the β-sheet that comprises part of this core (*23*). Spectroscopic studies indicate that the signal is transduced through the protein though reorganization of the hydrogen-bonding network surrounding the chromophore following light-induced adduct formation and uptake of a proton at the N5 atom of FMN (*24*, *25*).

In order to explore the mechanism of redox state recognition and signal transduction within this class of flavin-based sensor proteins, we have determined the crystal structure of the redox sensor domain of *Av*NifLF at 1.04 Å resolution. This structure reveals distinct structural differences between the FAD-based *Av*NifLF domain and related FMN-based photosensor proteins.

[1] The term "*l*ight *o*xygen *v*oltage (LOV) domain" was originally used to describe a subgroup of the large PAS domain superfamily characterized by elevated sequence homology. The term LOV domain has also been used in a more restricted sense to describe a subclass of FMN-based photoreceptors of the PAS domain family which bind flavin and exhibit cysteinyl adduct photochemistry (*1*). Technically, the *o*xygen sensors NifL and AER and the *v*oltage-sensitive N-terminal domain of the human potassium channel HERG are also members of the broader class of LOV domains. For clarity, we use the restricted LOV definition of Crosson et al. (*1*) and do not refer to nonphotoreceptor PAS domains as LOV domains.

MATERIALS AND METHODS

Protein Expression and Crystallization. *Av*NifLF was expressed as described previously (*26*). This construct encodes residues 1−140 of the NifL protein plus a 23-residue N-terminal extension with a 6-His tag. Protein was purified using nickel-NTA affinity resin (Qiagen) and gel filtration chromatography using Sephacryl S-200 resin in 300 mM NaCl, 50 mM Tris, pH 8.0, and 5 mM imidazole and elutes as a tetramer of ~60 kDa. Protein purity was judged by SDS−PAGE. The N-terminal 6-His tag and extension were retained on the protein prior to crystallization trials. Crystals were grown by the hanging drop vapor diffusion method against a reservoir of 2.25 M ammonium sulfate and 5% ethanol using a protein concentration of 7 mg/mL in 10 μL drops with a 1:1 protein to mother liquor ratio. These conditions yield crystals in the rhombohedral *R*32 space group similar to those reported previously (*26*). As *Av*NifLF oxidizes rapidly in the presence of oxygen, crystals were grown in the oxidized state. Crystals were only obtained in unbuffered conditions; indeed, attempts to stabilize the pH prohibited crystal growth. Crystals took 3 months to grow and were often of very large size ($1000 \times 1000 \times 300$ μm). A platinum heavy atom derivative was obtained by soaking the native crystals in 10 mM ammonium tetrachloroplatinate for 1 month. Crystals were soaked in a cryoprotectant of 2.25 M ammonium sulfate, 5% ethanol, and 17% glycerol and flash frozen in a 100 K nitrogen gas stream prior to X-ray data collection.

Data Collection and Reduction. X-ray oscillation diffraction data were collected on a MAR165 CCD detector at BioCARS beamline ID-B, sector 14 at the Advanced Photon Source (APS), Argonne, IL. Native data were collected in two passes from a single crystal: a high-resolution pass of 0.3° oscillations and a low-resolution pass of 0.5° oscillations. An X-ray energy of 15 keV (0.8266 Å wavelength) was used to collect high-resolution data. Diffraction images were integrated and scaled using the HKL2000 program suite (*27*). Experimental phases were obtained by three-wavelength MAD from a platinum derivative. SOLVE was used to locate three platinum atoms within the asymmetric unit and calculate initial phases to 2.7 Å resolution (*28*). Data statistics are presented in Table 1.

Model Building and Refinement. An initial model of *Av*NifLF was autobuilt from experimental phases using RESOLVE (*29*). The platinum derivative was not isomorphous with data from native crystals so a partial initial model was placed into the native data by molecular replacement using Phaser (*30*). Automated model building was carried out using ARP/wARP (*31*) with all native data to 1.04 Å resolution. Side chains were added manually using the program XFIT (*32*). During model building it became apparent from the electron density that a portion of one of the two monomers in the asymmetric unit, denoted monomers A and B, exhibited disorder within the crystal. Reexamination of the X-ray diffraction images confirmed the presence of a low-resolution weakly diffracting superlattice in the diffraction data, arising from a difference in noncrystallographic symmetry in adjacent asymmetric units. Despite its presence, we were able to completely build and satisfactorily refine both the A and B monomers. Anisotropic refinement was conducted using Refmac5 (*33*), gradually relaxing stereo-

Table 1: Data Collection and Refinement Statistics for *Av*NifLF in Space Group *R*32[a]

data statistics				
data set	native	Pt peak	Pt inflection	Pt remote
unit cell dimensions (Å)	$a = b = 68.11$, $c = 302.06$	$a = b = 67.90$, $c = 313.17$		
solvent content (%)	39.61			
wavelength (Å)	0.8266	1.072	1.074	1.041
mosaicity (deg)	0.20	0.27	0.29	0.27
diffraction limit (Å)	1.04	2.5	2.5	2.5
completeness (%) (last shell)	95.7 (70.0)	99.6 (100)	99.5 (100)	99.6 (100)
unique reflections	124275	10056	10051	10056
redundancy	6.36	10.8	10.8	10.8
$I/\sigma I$ (last shell)	36.7 (2.0)	67.6 (24.3)	67.9 (24.1)	67.6 (23.4)
R_{sym} (%) (last shell)	4.2 (41.3)	4.9 (9.7)	5.3 (9.7)	4.5 (9.7)
Pt sites		4	4	4
overall figure of merit to 2.7 Å resolution	0.69[b]			
refinement				
R_{work}, R_{free} (%)	15.4, 18.6			
RMSD from ideal bond lengths (Å)	0.027			
RMSD from ideal bond angles (deg)	3.46			
Ramachandran plot preferred, allowed (%)	93.8, 6.2			

[a] The last resolution shell spans 1.08−1.04 Å for native data and 2.59−2.5 Å for the platinum MAD datasets. $R_{sym}(I) = \sum_h\sum_i|I_i - I|/\sum_h\sum_i I$, where I is the mean intensity of the i observations of reflection h. $R_{work} = \sum|F_o - F_c|/\sum|F_o|$, where F_o and F_c are the observed and calculated structure factors, respectively. R_{free} is calculated from a randomly selected subset of the data (10%) excluded from refinement. [b] The overall figure of merit increased to 0.81 after density modification.

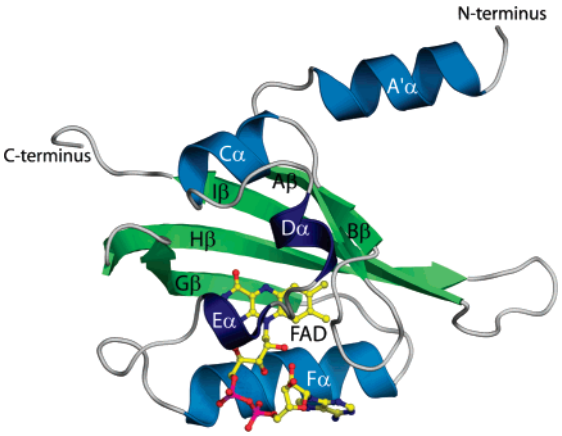

FIGURE 1: Ribbon diagram of the *Av*NifLF structure. Secondary structural elements are colored green for β-sheet, light blue for α-helix, and dark blue for 3_{10} helices.

chemical restraints. Solvent atoms were added initially using Arp/wArp and later manually in XFIT. Four sulfate ions are visible in the structure. These were modeled accordingly and refined at partial occupancy. All water molecules were refined with an occupancy of 1.0. Alternate side chain conformations were built for residues Asn75 and Met132 in the A monomer and Met132 in the B monomer. Data collection and refinement statistics are summarized in Table 1. Values of the *R*-factor (R_{free}) for the structure are 15.4% (18.6%), somewhat higher than expected for an excellent structure at 1.04 Å resolution, and are presumably a consequence of the crystal disorder and the superlattice this creates in the diffraction pattern. Side chains for five solvent-exposed residues in the B chain (Arg52, Gln92, Lys107, Gln138, and Arg134) could not be adequately modeled and were refined with occupancy set to 50% or 0%. Figures were created using the program Pymol (*34*, *35*). In Figure 1 we use the naming convention for secondary structural features in PAS domains introduced for the structure of FixL (*36*) as it is simpler than the current nomenclature for LOV domains (*37*) and facilitates comparison between PAS domain structures.

Structures were aligned using the program top from the CCP4 suite of programs (*33*). The sequence of the *Av*NifLF protein (Accession Number CAA46044) was aligned using ClustalW (http://www.ebi.ac.uk/clustalw/) to the PAS domain sequences of *E. coli* AER and Dos (Accession Numbers P50466 and P76129, respectively), *Adiantum capillus-veneris* Phy3 LOV1 and LOV2 (Accession Number BAA36192), *Homo sapiens* HERG (Accession Number BAA37096), wc-1, wc-2, and vivid of *Neurospora crassa* (Accession Number XP_959777, XP_063819, and AAK08514, respectively), FixL from *Bradyrhizobium japonicum* and *Sinorhizobium meliloti* (Accession Numbers CAA40143 and CAA79897, respectively), and photoactive yellow protein (PYP) from *Halorhodospira halophila* (Accession Number AAB28014). Sequences were shaded at a 50% identity and similarity cutoff using Boxshade (http://www.ch.embnet.org/). Cavities and tunnels were identified within the *Av*NifLF structure using the program Voidoo (*38*) and visualized using Pymol.

RESULTS

Structure of a FAD-Based Redox Sensor. The structure of *Av*NifLF at 1.04 Å resolution reveals the characteristic α/β PAS domain fold (*11*) in which a single molecule of the oxidized FAD cofactor is noncovalently bound within the core of the protein (Figure 1). The structure reveals residues 22−140 in monomer A and residues 21−139 in monomer B. Although the initial 21 N-terminal residues of the protein and a 23-residue N-terminal affinity tag were expressed, purified, and are present during crystallization, no electron density corresponding to them is visible. These residues are either completely disordered in the crystal or proteolyzed during crystallization. As predicted, the structure of the *Av*NifLF backbone is similar to the structures of photoreceptor PAS/LOV domains from higher plants and green algae (*37*, *39*), both of which bind FMN as their chromophore. The structural similarity determined by structure alignment between *Av*NifLF, photoreceptor LOV domains (PDB codes 1N9L and 1G28), and a number of other PAS domain structures is listed in Table 2.

Table 2: Comparison of the Sequence and Structure of *Av*NifLF to Known PAS Domain Crystal Structures[a]

PAS domain, organism	PDB ID code	sequence identity (%)	structural diversity
LOV1, *Chlamydomonas reinhardtii*	1N9L	29.0	1.82
LOV2, *A. capillus-veneris*	1G28	23.7	2.09
HERG, *H. sapiens*	1BYW	24.0	2.39
*Sm*FixLH, *S. meliloti*	1EW0	28.8	2.60
*Bj*FixLH, *B. japonicum*	1LSW	24.0	2.63
*Ec*DosH, *E. coli*	1S66	25.9	3.19
Pph PYP, *Rhodospirillum centenum*	1MZU	13.9	3.74
PYP, *Ectothiorhodospira halophila*	2PHY	18.9	3.85
CitA, *Klebsiella pneumoniae*	1P0Z	18.0	5.31

[a] Sequence identity is defined as the percent of residues identical to those in *Av*NifLF. Structural diversity is defined as (Cα RMSD)($N_{Av\text{NifLF}}/N_{\text{fit}}$)^2. $N_{Av\text{NifLF}}$ is the total number of residues in the *Av*NifLF monomer (118), and N_{fit} is the number of spatially matched Cα atoms (less than 3.8 Å distant). For dimeric PAS structures (*Ec*DosH and *Sm*FixLH), comparison was made only between monomers.

FAD Binding within the PAS Domain. The PAS domain has been shown to bind a wide array of chemically diverse prosthetic groups, but the structure of *Av*NifLF provides the first structural example containing FAD. Binding of its isoalloxazine ring is stabilized by hydrogen bonds from the side chain of Asn102 to the N3 and O4 atoms of FAD, as also occurs in the coordination of FMN in LOV1 and LOV2 of plant phototropins (*37*, *39*). Binding of the ribose and adenine portions of the FAD cofactor (absent in FMN-based structures) is stabilized by interactions with the side chains of residues Trp87 and Arg80 (Figure 2). The side chain of Trp87 forms a hydrophobic stacking interaction with the base moiety of the adenine and also forms hydrogen bonds to both the 2- and 3-hydroxyl groups of the ribityl chain of the FAD through the nitrogen atom of the indole ring. The positively charged side chain of Arg80 in *Av*NifLF binds to the O1P phosphate oxygen, a common motif in flavoproteins. We observe two different conformations of the FAD ribose in the A and B monomers. In the A monomer, the δ-nitrogen atom of Asn69 is hydrogen bonded to the AO2* oxygen atom of the ribose moiety of the FAD group. In the B monomer, the ribose is in an alternate conformation which facilitates the molecular packing within the crystal lattice. A stacking interaction between Trp87 and the adenine moiety of the FAD of the B-monomer forms a four-base stack with a neighboring, symmetry-related adenine and the side chain of its Trp87 residue. This orientation results in an alternate conformation of the FAD which lacks the Asn69 to AO2* hydrogen bond.

A notable feature of the FAD binding pocket is the presence of a glutamate residue, Glu70, at a location structurally equivalent to that of the critical cysteine residue of photosensor LOV domains on the *si* face of the isoalloxazine ring (Figure 2). The carboxylic acid group of the Glu70 side chain is 3.4 Å from the N5 atom of the FAD. In photosensor LOV domains, covalent attachment of this cysteine to FMN initiates the structural change within the molecule upon exposure to blue light (*22*). In *Av*NifLF the corresponding glutamate is directly involved in the hydrogen bond network within the FAD cavity. This hydrogen-bonding network may be sensitive to the redox state of the FAD (discussed below).

AvNifLF Contains Two Buried Water Molecules and an Access Tunnel. The most significant differences between *Av*NifLF and photoreceptor LOV domains are found not in the coordinating residues of the FAD group but within the interior of the domain. Adjacent to the buried side of the FAD group, cavities are present within the core (Figure 3). Two buried water molecules are positioned in a cavity in direct proximity to the N5 and C4 atoms of the FAD, linked to the surface by a pathway from the internal cavity through the protein. The two cavities are separated by the side chains of Glu70, Phe54, and Leu73; the two water molecules are completely enclosed within the protein and are not coordinated with the hydrogen bond network of the protein solvent shell. Analogous internal water has not been observed in structures of other PAS domain proteins. The two molecules, denoted Wat2 and Wat9 in the A monomer and Wat47 and Wat319 in the B monomer, are located within a network of hydrogen bonds in the FAD cavity. This network includes the side chains of residues Ser39, Glu70, Asn102, Tyr110, and His133, which line the cavity, and the N5 and O4 atoms of the FAD. Although our crystallographic resolution of 1.04 Å is not sufficient to directly detect the electron density of hydrogen atoms, it is sufficient to distinguish C from N from O and thus to identify unambiguously the orientation of side chains and to predict the locations of hydrogen atoms with confidence and hydrogen bond distances with precision

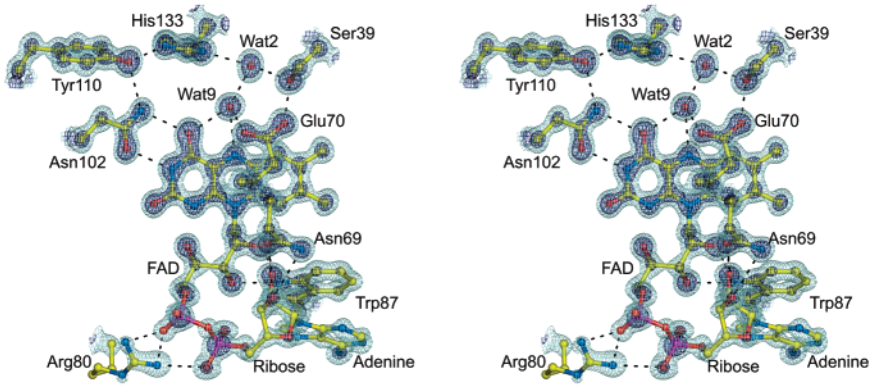

FIGURE 2: A $2F_o - F_c$ electron density map of the FAD cofactor and its coordinating residues, shown as a ball and stick model. Hydrogen bonds are denoted by green dashed lines. Orientation as in Figure 1. Note that at 1.04 Å resolution the quality of the electron density is sufficient to distinguish carbon from nitrogen atoms, e.g., in the side chains of Asn69 and Asn102. Electron density is contoured at 2σ (light blue) and 4.5σ (dark blue) where σ is the RMS value of ρ across the asymmetric unit.

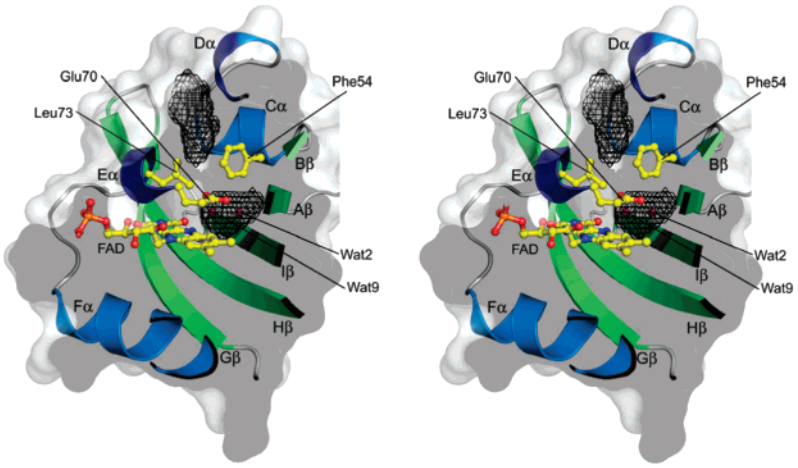

FIGURE 3: The van der Waals surface of *Av*NifLF (gray transparent surface) showing the internal cavity and solvent access channel into the core of *Av*NifLF identified with the program VOIDOO and depicted as a in black wire frame. Also shown are the two internal water molecules (depicted as dark red spheres), the FAD, the side chains of Glu70, Leu73, and Phe54 which separate the two cavites, and the protein backbone in ribbon representation.

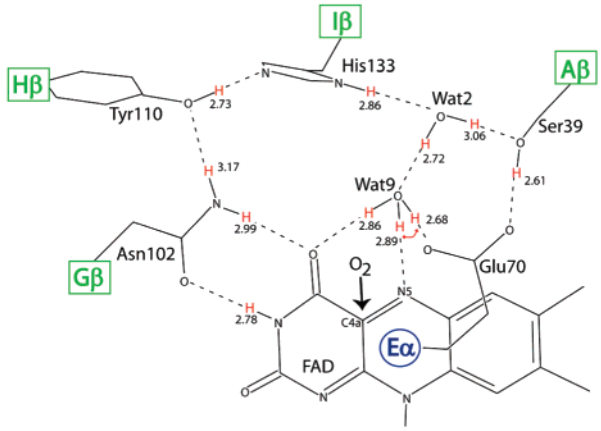

FIGURE 4: Hydrogen bonding within the oxidized *Av*NifLF flavin binding pocket. Hydrogen atoms are depicted in red; hydrogen bond lengths (from donor to acceptor) in angstroms are noted in black. The secondary structure elements to which residues belong are colored as in Figure 1. Note that Wat9 is surrounded by three hydrogen bond acceptors and only one donor in the oxidized state; equilibrium between donors is depicted with a red arrow. C4a, the site of oxidation by molecular oxygen, is indicated with a black arrow.

(Figure 4). These locations are critical to understanding redox-mediated signaling.

A Conserved Dimerization Motif. Full-length NifL is tetrameric in solution, as is *Av*NifLF. However, no tetramer of *Av*NifLF can be unambiguously identified in our *R*32 crystal form. It is likely that the tetramer of NifL is a homodimer of the dimeric complex in our crystal structure, but the nature of this tetrameric interaction is unclear. The dimer of *Av*NifLF molecules in the asymmetric unit is nearly identical in quaternary structure to the crystal structures of the heme-based PAS domains of the protein Dos from *E. coli* (*Ec*DosH; PDB codes 1S66 or 1V9Y) and FixL from *S. meliloti* (*Sm*FixLH; PDB code 1D06) (*40*−*42*) (Figure 5A). As in *Ec*DosH and *Sm*FixLH, the *Av*NifLF dimer is stabilized by an amphipathic helix spanning residues 23−34 immediately N-terminal to the core of the PAS domain. Since this helix is conserved in certain other PAS domains, we denote it A′α to conform with the naming scheme for secondary structural elements in PAS domains (*36*). In the *Av*NifLF dimer, the amphipathic A′α helices interact via the side chains of Pro24, Ile26, Phe27, and Val31 and the hydrophobic portion of the side chain of Arg28 to form a leucine zipper-like motif (*41*) (Figure 5B). The C-terminal end of each A′α helix in *Av*NifLF also packs onto the N-terminal end of helix Cα. This interaction is stabilized by both helix dipole interactions and hydrogen bonds between the side chain of Asn51 and the backbone atoms of residue Val31 to form a larger α-helix that, most unusually, is continuous in structure yet discontinuous in protein sequence. Within the dimer, the amphipathic A′α helix packs against the hydrophobic surface of the *β*-sheet of the opposing monomer and, in particular, with Ile40 in the A*β* strand and Leu130 in the I*β* strand. These interactions result in a tightly packed hydrophobic core between the two monomers which buries 2066 Å^2 of solvent-accessible surface area.

*Sm*FixL is an oxygen sensor and is a member of the large class of two-component system sensor histidine kinases (*43*). As such, it is similar to NifL, which is homologous to (but not a member of) the large class of bacterial two-component sensor histidine kinases. *Ec*Dos is a PAS-regulated phosphodiesterase (*44*) that, with the exception of their common PAS domains, is not related in domain structure to either FixL or NifL. Both *Sm*FixLH and *Ec*DosH bind an iron protoporphyrin IX (heme) prosthetic group and show modest sequence homology with flavin-binding LOV domain photoreceptors (Table 2). Nevertheless, we were surprised to see that these different PAS domains utilize the same mode of dimerization based on the A′α helix. To explore the possible generality of this observation, we aligned the sequences of a number of related PAS proteins (Figure 6A) to reveal a candidate, highly amphipathic N-terminal helix in the FMN-based photoreceptors phy3 LOV1 and LOV2 (*37*), white collar 1 (wc-1) and its signaling partner white collar 2 (wc-2), the FMN-based photoreceptor vivid (vvd), the FAD-based aerotaxis receptor AER, and [as first noted by Rajagopal (*45*)] the N-terminal PAS domain of HERG (Figure 6B). Thus, we advance our first proposal: FMN- and FAD-based PAS sensors employ the structural dimer-

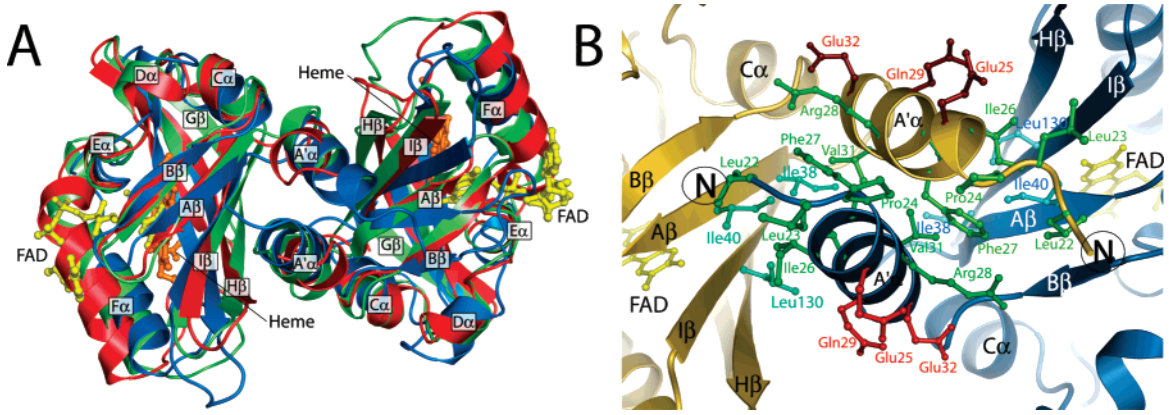

FIGURE 5: (A) Structural alignment of the dimeric structures of *Av*NifLF (blue), *Ec*DOSH (green), and *sm*FixLH (red). The FAD of *Av*NifLF and the heme of *Ec*DosH are shown in space-filling representation. For clarity, the heme and the short additional N-terminal helix of *sm*FixLH are omitted. (B) Packing of the amphipathic N-terminal A′α helix of *Av*NifLF on the *β*-sheet within the PAS dimer. The orientation and secondary structure elements of *Av*NifLF are as in panel A. Hydrophobic residues of the A′α helix and the *β*-sheet involved in packing interactions are shown in green and cyan, respectively. The hydrophilic/charged residues of the A′α helix are shown in red. Backbone atoms of *Av*NifLF are depicted as gold and blue ribbons for the A and B monomers, respectively.

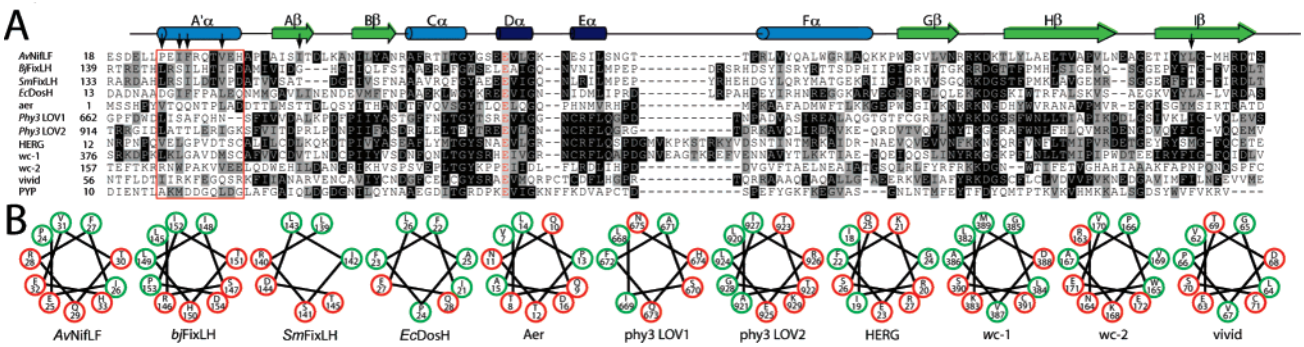

FIGURE 6: (A) Sequence alignment of the PAS domains of *A. vinelandii* NifL, maidenhair fern Phy3 domains LOV1 and LOV2, *N. crassa* wc-1, wc-2, and vivid, *E. coli* AER and Dos, the heme-based PAS of FixL from *B. japonicum* and *S. meliloti*, and *H. halophila* PYP. Secondary structure elements of *Av*NifLF are depicted as a cartoon above the sequences and colored as in Figure 1. Sequence identity is shaded in black and similarity in gray, with a 50% threshold. The A′α helix of *Av*NifLF and putative helices of the other proteins are outlined in a red rectangle. Amino acids which lie within the hydrophobic dimerization interface are noted with an arrow. (B) Helical wheel representations of the observed amphipathic N-terminal helices from the dimeric structures of *Av*NifLF, *Ec*DosH (PDB code 1S66), and *Sm*FixLH (PDB code 1EW0) and structural predictions of N-terminal helices of aer, HERG, LOV1, LOV2, wc-1, wc-2, and vivid, based on the sequence alignment with *Av*NifLF in panel A. Hydrophobic residues are shown in green; hydrophilic, in red.

ization motif of an amphipathic N-terminal helix, in common with those of heme-based PAS sensors. However, PAS dimerization in this manner may be more general; our first proposal also extends to non-flavin-based PAS domains such as HERG and wc-2.

Crystal structures are available for the proteins *Adiantum phy3* LOV2, *Chlamydomonas* phot LOV1, and human HERG but not for the remaining PAS domains noted above. Dimers as described for *Av*NifLF were not observed in the structures of LOV1 and LOV2 (PDB ID 1G28 and 1N9L, respectively). Residues N-terminal to the core PAS domain were not present during crystallization of these domains. In the HERG crystal structure, however, residues of the candidate N-terminal helix are present in the crystal, but only disordered density is visible (*46*). Nevertheless, a very similar dimer to that described for *Av*NifLF, *Ec*DosH (*40*, *42*), and *Sm*FixLH (*41*) is observed between the single HERG molecule of the asymmetric unit and a symmetry-related molecule in the crystal lattice.

The heterodimeric solution structures of the aryl hydrocarbon receptor nuclear translocator (ARNT) and the hypoxia-inducible factor alpha (HIF1-α) were recently determined using NMR methods (*47*). The ARNT-HIF-α heterodimer employs an interdomain association of hydrophobic antiparallel *β*-sheets, analogous to that of *Av*NifLF, *Ec*DosH, or *Sm*FixLH. Mutations in this *β*-sheet surface of HIF-2α disrupt this interaction in vitro and substantially alter the in vivo response to hypoxia (*48*). However, none of the structures of ARNT, the ARNT-HIF-α heterodimer, or HIF-2α contain N-terminal amphipathic helices such as those observed in *Av*NifLF, *Ec*DOS, and *Sm*FixLH. Furthermore, when the N-terminal sequences of the ARNT, HIF-1α, and HIF-2α domains are aligned to sequences from known PAS dimers, no significant homology is found, nor are any candidate N-terminal amphipathic helices revealed. This finding is discussed further below.

DISCUSSION

Sensing Oxygen Indirectly through the Redox State. In order for NifL to sense and respond to changes in oxygen concentration, the protein must be able both to recognize oxygen and to generate a structural signal that can be detected by other components of the signaling pathway. Though the FAD is buried within the core of *Av*NifL, the structure

provides a facile pathway for access by oxygen to the C4a and N5 atoms of the bound FAD. The solvent access channel, the internal solvent-filled cavity, and the FAD may facilitate the recognition of oxygen by providing dissolved diatomic oxygen access to the C4a atom of the isoalloxazine ring, the site of FAD oxidation (Figure 4). The C4a atom is also the site of signal generation in related photoreceptor LOV domains via light-dependent covalent attachment of a nearby cysteine side chain (*22*, *49*). Oxidation of FAD by diatomic oxygen takes place via the attack of oxygen at the C4a carbon atom of the isoalloxazine ring, followed by the formation of a transient hydroperoxy intermediate species (*50*), and, finally, hydrolysis, protonation of the FAD at atoms N5 and N1, and release of peroxide. The cavity adjacent to the FAD ring can accommodate the formation of the hydroperoxy intermediate species within the protein and provide an exit pathway for hydrogen peroxide (Figure 3). Similar "oxygen access tunnels" have been reported in the atomic resolution structure of FAD-based cholesterol oxidase (*49*), in which the reoxidation of FAD by molecular oxygen and subsequent release of peroxide, the so-called oxidative half-reaction (*51*), is a critical step in enzyme turnover. Access tunnels or channels are dependent on the conformational dynamics of side chain residues (*49*) and may appear as a series of transiently occupied cavities, such as those found in the oxygen transport/storage protein myoglobin (*52*). We propose that the channels in *Av*NifLF act similarly to those in oxidases; the side chains which line the channels, as well as the residues of the flavin pocket (Phe54, Glu70, and Leu73), transiently open the channels by thermal motion and, thus, facilitate redox sensing. The side chain of Glu70 is poised in an ideal location within the cavity to interact with a hydroperoxy intermediate after oxygen reacts at the C4a atom. Glu70 may facilitate the formation of this species, effectively catalyzing the oxidation of the FAD or the hydrolysis of the hydroperoxy intermediate. Alternatively, hydrolysis may be accomplished by the nearby coordinated water molecule, Wat9/Wat319, within the protein. The surrounding side chains such as Tyr110, Ser39, and His133 provide a network of hydrogen bond donors and acceptors which may facilitate the uptake and release of protons at N5 of the FAD during oxidation and reduction of the FAD group and thereby facilitate the redox switch.

Redox-Induced Structural Change: Generating and Transmitting a Signal. After *Av*NifLF encounters oxygen and a change in redox state occurs, that information must be transmitted through the molecule in the form of a structural signal. Structural changes have been observed in the β-strands of the related PAS domain phy3 LOV2 by Nozaki and colleagues, who suggest that adduct formation is accompanied by rearrangement of the hydrogen bonding of water molecule(s) near the chromophore (*25*). A glutamine side chain forms a hydrogen bond with the N5 atom of the FMN, which becomes protonated in response to light. This glutamine reorients its hydrogen bond interactions upon adduct formation (*22*, *24*, *25*), thus initiating the propagation of the structural signal through the protein.

The structure of *Av*NifLF suggests that a similar mechanism is at work upon redox change. Reorganization of the hydrogen-bonding interactions of the two bound water molecules within the protein may play a role analogous to that of the glutamine residue of photoreceptors. Protonation/deprotonation of the N5 atom of the FAD upon change in redox state necessitates reorganization of the hydrogen bond network within the protein, which constitutes a structural signal (Figure 4). The side chains of residues Glu70, His133, and Ser39 are the most likely participants. Changes in the positions of these side chains and the two water molecules within the protein have been observed upon prolonged illumination of *Av*NifLF by the X-ray beam, possibly arising from photoreduction (*53*, *54*). Glu70 is located directly over the N5 atom of the FAD, poised to accept a hydrogen bond from a protonated N5 atom, and is accessible to solvent via a protein channel. Glu70 is also hydrogen-bonded to the side chain β-sheet residue Ser39, whose side chain makes a second hydrogen bond with one of the buried water molecules, Wat9/Wat319. Thus Ser39 is sensitive to changes in structure that originate in protonation of N5 and alter hydrogen bonding by the side chain of Glu70 and Wat9/Wat319. Furthermore, Ser39 is located in the core β-sheet in a structural position analogous to that implicated in the signaling processes of other PAS proteins such as the heme domain of FixL (*55*), the N-terminal domain of the human potassium channel (HERG) (*46*), human hypoxia inducible factor 2 (HIF2-α) (*56*), and photoreceptor LOV domains (*23*, *25*).

We therefore advance our second proposal: the signaling mechanism in these related light- or redox-sensitive, flavin-based PAS domains employs a common strategy, the signal-dependent rearrangement of internal hydrogen bonds.

Anderson and colleagues have reported the structure of the FAD-based photoreceptor domain of the protein AppA, an antirepressor of photosynthetic gene transcription in *Rhodobacter sphaeroides* (*57*). The photoreceptor is a BLUF domain (*58*) whose ferredoxin-like tertiary structure differs completely from those of PAS domains. However, as in LOV domains and NifL, the AppA protein rearranges its hydrogen-bonding network to generate and transmit signal. The hydrogen-bonding network between the FAD N5 atom and a nearby conserved tryptophan side chain of the AppA BLUF domain is likely to be rearranged upon exposure to light and the transient gain of a proton at N5. Recent ultrafast spectroscopic studies support this model and propose a transiently protonated FAD semiquinone intermediate (*59*, *60*).

These data enable us to generalize our second proposal. Signal-dependent rearrangement of internal hydrogen bonds is a conserved mechanism for relaying structural signal from the N5 atom of a flavin to the surface of a sensor protein (here a β-sheet surface), independent of the overall tertiary structure of the protein (for example, PAS or BLUF).

How do conformational changes in the *Av*NifLF PAS domain modulate the binding affinity for NifA in a NifL tetramer? The *Av*NifLF domain is not required for the NifL−NifA interaction but is required to impart redox-regulated binding (*8*). Additionally, a critical mutation in *Av*NifL in the linker region between the PAS and C-terminal kinase-like domains blocks the ability of the protein to detect redox signals (*61*). Thus a plausible model for control of NifA binding requires action at a distance: a redox-dependent exposure of a binding surface on the *Av*NifL holoprotein driven by conformational changes within the homodimeric *Av*NifLF PAS domain. We therefore advance our third proposal: upon redox change, structural changes propagate

into the interface between the *Av*NifLF monomers, alter their affinity for each other, and cause a quaternary structural change which ultimately modulates binding affinity of the Q-linker (*62*) and C-terminal domains of NifL for the NifA protein. This model is supported by studies of other PAS domain dimers (*40*, *42*) which suggest quaternary, signal-dependent conformational changes driven by structural changes along the β-strands of the protein (*40*, *42*, *55*). This scissor-like quaternary structural change has been proposed (*40*, *55*) to alter the conformation of downstream enzymatic domains in order to regulate their activity. In the case of NifL, the binding affinity of the C-terminal kinase-like domain for NifA would be regulated in an analogous manner to the mechanism proposed for its evolutionary cousins, the sensor histidine kinases of two-component systems.

Additional clues to the redox control of binding affinity come from the work of Harper and colleagues (*23*), who identified light-sensitive conformational changes in an amphipathic Jα helix immediately C-terminal to the core PAS domain in the flavin-based photoreceptor LOV2. Mutations in this region lead to inability of the LOV2 PAS domain to regulate kinase activity (*63*). This light-sensitive Jα helix of the LOV2 helix packs against the surface of the β-sheet of the PAS domain. Given the high sequence and structural homology between *Av*NifLF and LOV2, a possible mechanism may involve the reorganization of hydrogen bonds within *Av*NifLF to exhibit a similar redox-dependent C-terminal "helix swap" within the NifL holoprotein in order to produce the type of conformational changes described above (see also Figure 9 of ref *7* and Figure 5 of ref *63*). Indeed, the sequence of *Av*NifL has a region spanning residues 186−202 that has significant sequence identity to the amphipathic C-terminal Jα helices of photoreceptor LOV2 domains. However, this putative helix in *Av*NifL is located a significant distance (45 amino acids) C-terminal to the PAS domain, and its role, if any, must be investigated further.

It should be noted that both the scissor-like and helix swap mechanisms are necessarily distinct from the strategy employed by the ARNT/HIF proteins, for which dynamic homo- and heterodimerization between ARNT, HIF-1α, and HIF-2α is critical for proper regulation of their C-terminal DNA binding domains. This mechanistic difference is a plausible explanation for the observed differences in the dimeric structures, namely, the absence of amphipathic N-terminal A′α helices. In contrast to the ARNT and HIF proteins, activity of NifL is not regulated by changes in oligomerization state; the protein is found as a tetramer under either oxidizing or reducing conditions in both the isolated PAS domain and the full-length protein. The hydrophobic leucine zipper-like motif between the β-sheet side chains and the A′α helices is likely to contribute substantially to the stability of this intersubunit interaction. The lack of an N-terminal amphipathic helix in ARNT/HIF-1α and HIF-2α PAS dimers may effectively free these individual domains to allow dynamic dimerization and dissociation-based regulation to occur at a physiologically relevant concentration and time scale. Alternatively, the A′α helix may only be ordered within the intact protein dimer and could be detected by docking structures determined from monomeric PAS domains.

Three common elements for signal transduction are thus evident within a broad range of sensory PAS domains: the generation of information by prompt reorganization of an internal hydrogen-bonding network in response to signal; the transmission of that information across the β-sheet; and the alteration of its surface to modify its affinity for, and thus affect the conformation of, an N- and/or C-terminal helix which lies adjacent to the PAS domain core. These specific conformational changes are adapted to the diverse purposes of full-length proteins.

ACKNOWLEDGMENT

J.K. thanks Spencer Anderson and the staff of BioCARS for assistance with data collection and Sean Crosson for valuable discussion. M.H. acknowledges fruitful discussions with Jacques Vervoort at Wageningen University.

REFERENCES

1. Crosson, S., Rajagopal, S., and Moffat, K. (2003) The LOV domain family: photoresponsive signaling modules coupled to diverse output domains, *Biochemistry 42*, 2−10.
2. Hill, S. (1992) Physiology of nitrogen fixation in free-living heterotrophs, in *Biological Nitrogen Fixation* (Stacey, G. S., Burris, R. H., and Evans, H. J., Eds.) pp 87−134, Chapman and Hall, New York.
3. Maier, R. J., and Moshiri, F. (2000) Role of the *Azotobacter vinelandii* nitrogenase-protective shethna protein in preventing oxygen-mediated cell death, *J. Bacteriol. 182*, 3854−3857.
4. Moshiri, F., Kim, J. W., Fu, C., and Maier, R. J. (1994) The FeSII protein of *Azotobacter vinelandii* is not essential for aerobic nitrogen fixation, but confers significant protection to oxygen-mediated inactivation of nitrogenase in vitro and in vivo, *Mol. Microbiol. 14*, 101−114.
5. Poole, R. K., and Hill, S. (1997) Respiratory protection of nitrogenase activity in *Azotobacter vinelandii*—roles of the terminal oxidases, *Biosci. Rep. 17*, 303−317.
6. Martinez-Argudo, I., Little, R., Shearer, N., Johnson, P., and Dixon, R. (2004) The NifL-NifA System: a multidomain transcriptional regulatory complex that integrates environmental signals, *J. Bacteriol. 186*, 601−610.
7. Gilles-Gonzalez, M. A., and Gonzalez, G. (2005) Heme-based sensors: defining characteristics, recent developments, and regulatory hypotheses, *J. Inorg. Biochem. 99*, 1−22.
8. Money, T., Jones, T., Dixon, R., and Austin, S. (1999) Isolation and properties of the complex between the enhancer binding protein NIFA and the sensor NIFL, *J. Bacteriol. 181*, 4461−4468.
9. Woodley, P., and Drummond, M. (1994) Redundancy of the conserved His residue in *Azotobacter vinelandii* NifL, a histidine autokinase homologue which regulates transcription of nitrogen fixation genes, *Mol. Microbiol. 13*, 619−626.
10. Taylor, B. L., and Zhulin, I. B. (1999) PAS domains: internal sensors of oxygen, redox potential, and light, *Microbiol. Mol. Biol. Rev. 63*, 479−506.
11. Hefti, M. H., Francoijs, K. J., de Vries, S. C., Dixon, R., and Vervoort, J. (2004) The PAS fold: a redefination of the PAS domain based upon structural prediction, *Eur. J. Biochem. 271*, 1198−1208.
12. Hill, S., Austin, S., Eydmann, T., Jones, T., and Dixon, R. (1996) *Azotobacter vinelandii* NIFL is a flavoprotein that modulates transcriptional activation of nitrogen-fixation genes via a redox-sensitive switch, *Proc. Natl. Acad. Sci. U.S.A. 93*, 2143−2148.
13. Schmitz, R. A. (1997) NifL of *Klebsiella pneumoniae* carries an N-terminally bound FAD cofactor, which is not directly required for the inhibitory function of NifL, *FEMS Microbiol. Lett. 157*, 313−318.
14. Austin, S., Buck, M., Cannon, W., Eydmann, T., and Dixon, R. (1994) Purification and in vitro activities of the native nitrogen fixation control proteins NifA and NifL, *J. Bacteriol. 176*, 3460−3465.
15. Lee, H. S., Narberhaus, F., and Kustu, S. (1993) In vitro activity of NifL, a signal transduction protein for biological nitrogen fixation, *J. Bacteriol. 175*, 7683−7688.

16. Macheroux, P., Hill, S., Austin, S., Eydmann, T., Jones, T., Kim, S. O., Poole, R., and Dixon, R. (1998) Electron donation to the flavoprotein NifL, a redox-sensing transcriptional regulator, *Biochem. J. 332* (Part 2), 413−419.
17. Little, R., Hill, S., Perry, S., Austin, S., Reyes-Ramirez, F., Dixon, R., and Macheroux, P. (1999) *Properties of NifL, a Regulatory Flavoprotein Containing a PAS Domain*, pp 737−740, Rudolf Weber, Berlin, Germany.
18. Repik, A., Rebbapragada, A., Johnson, M. S., Haznedar, J. O., Zhulin, I. B., and Taylor, B. L. (2000) PAS domain residues involved in signal transduction by the Aer redox sensor of *Escherichia coli*, *Mol. Microbiol. 36*, 806−816.
19. Christie, J. M., Reymond, P., Powell, G. K., Bernasconi, P., Raibekas, A. A., Liscum, E., and Briggs, W. R. (1998) *Arabidopsis* NPH1: a flavoprotein with the properties of a photoreceptor for phototropism, *Science 282*, 1698−1701.
20. Huala, E., Oeller, P. W., Liscum, E., Han, I. S., Larsen, E., and Briggs, W. R. (1997) *Arabidopsis* NPH1: a protein kinase with a putative redox-sensing domain, *Science 278*, 2120−2123.
21. Salomon, M., Christie, J. M., Knieb, E., Lempert, U., and Briggs, W. R. (2000) Photochemical and mutational analysis of the FMN-binding domains of the plant blue light receptor, phototropin, *Biochemistry 39*, 9401−9410.
22. Crosson, S., and Moffat, K. (2002) Photoexcited structure of a plant photoreceptor domain reveals a light-driven molecular switch, *Plant Cell 14*, 1067−1075.
23. Harper, S. M., Neil, L. C., and Gardner, K. H. (2003) Structural basis of a phototropin light switch, *Science 301*, 1541−1544.
24. Iwata, T., Nozaki, D., Tokutomi, S., Kagawa, T., Wada, M., and Kandori, H. (2003) Light-induced structural changes in the LOV2 domain of *Adiantum* phytochrome3 studied by low-temperature FTIR and UV-visible spectroscopy, *Biochemistry 42*, 8183−8191.
25. Nozaki, D., Iwata, T., Ishikawa, T., Todo, T., Tokutomi, S., and Kandori, H. (2004) Role of Gln1029 in the photoactivation processes of the LOV2 domain in *Adiantum* phytochrome3, *Biochemistry 43*, 8373−8379.
26. Hefti, M., Hendle, J., Enroth, C., Vervoort, J., and Tucker, P. A. (2001) Crystallization and preliminary crystallographic data of the PAS domain of the NifL protein from *Azotobacter vinelandii*, *Acta Crystallogr., Sect. D: Biol. Crystallogr. 57*, 1895−1896.
27. Otwinowski, Z., and Minor, W. (1997) Processing of X-ray diffraction data collected in oscillation mode, *Methods Enzymol. 276*, 307−326.
28. Terwilliger, T. C., and Berendzen, J. (1999) Automated MAD and MIR structure solution, *Acta Crystallogr., Sect. D: Biol. Crystallogr. 55*, 849−861.
29. Terwilliger, T. C. (2003) Improving macromolecular atomic models at moderate resolution by automated iterative model building, statistical density modification and refinement, *Acta Crystallogr., Sect. D: Biol. Crystallogr. 59*, 1174−1182.
30. Read, R. J. (2003) Pushing the boundaries of molecular replacement with maximum likelihood, *Acta Crystallogr., Sect. D: Biol. Crystallogr. 59*, 404−404.
31. Perrakis, A., Morris, R., and Lamzin, V. S. (1999) Automated protein model building combined with iterative structure refinement, *Nat. Struct. Biol. 6*, 458−463.
32. McRee, D. E. (1999) XtalView/Xfit−A versatile program for manipulating atomic coordinates and electron density, *J. Struct. Biol. 125*, 156−165.
33. Bailey, S. (1994) The Ccp4 Suite−Programs for Protein Crystallography, *Acta Crystallogr., Sect. D: Biol. Crystallogr. 50*, 760−763.
34. Carson, M. (1997) Ribbons−Macromolecular Crystallography, *Methods Enzymol. 277*, 493−505.
35. DeLano, W. L. (2002) Pymol, DeLano Scientific, San Carlos, CA.
36. Gong, W., Hao, B., Mansy, S. S., Gonzalez, G., Gilles-Gonzalez, M. A., and Chan, M. K. (1998) Structure of a biological oxygen sensor: a new mechanism for heme-driven signal transduction, *Proc. Natl. Acad. Sci. U.S.A. 95*, 15177−15182.
37. Crosson, S., and Moffat, K. (2001) Structure of a flavin-binding plant photoreceptor domain: insights into light-mediated signal transduction, *Proc. Natl. Acad. Sci. U.S.A. 98*, 2995−3000.
38. Kleywegt, G. J., and Jones, T. A. (1994) Detection, delineation, measurement and display of cavities in macromolecular structures, *Acta Crystallogr., Sect. D: Biol. Crystallogr. 50*, 178−185.
39. Fedorov, R., Schlichting, I., Hartmann, E., Domratcheva, T., Fuhrmann, M., and Hegemann, P. (2003) Crystal structures and molecular mechanism of a light-induced signaling switch: The Phot-LOV1 domain from *Chlamydomonas reinhardtii*, *Biophys. J. 84*, 2474−2482.
40. Kurokawa, H., Lee, D. S., Watanabe, M., Sagami, I., Mikami, B., Raman, C. S., and Shimizu, T. (2004) A redox-controlled molecular switch revealed by the crystal structure of a bacterial heme PAS sensor, *J. Biol. Chem.*
41. Miyatake, H., Mukai, M., Park, S. Y., Adachi, S., Tamura, K., Nakamura, H., Nakamura, K., Tsuchiya, T., Iizuka, T., and Shiro, Y. (2000) Sensory mechanism of oxygen sensor FixL from *Rhizobium meliloti*: crystallographic, mutagenesis and resonance Raman spectroscopic studies, *J. Mol. Biol. 301*, 415−431.
42. Park, H., Suquet, C., Satterlee, J. D., and Kang, C. (2004) Insights into signal transduction involving PAS domain oxygen-sensing heme proteins from the X-ray crystal structure of *Escherichia coli* Dos heme domain (Ec DosH), *Biochemistry 43*, 2738−2746.
43. Gilles-Gonzalez, M. A., Ditta, G. S., and Helinski, D. R. (1991) A haemoprotein with kinase activity encoded by the oxygen sensor of *Rhizobium meliloti*, *Nature 350*, 170−172.
44. Delgado-Nixon, V. M., Gonzalez, G., and Gilles-Gonzalez, M. A. (2000) Dos, a heme-binding PAS protein from *Escherichia coli*, is a direct oxygen sensor, *Biochemistry 39*, 2685−2691.
45. Rajagopal, S. (2004) Ph.D. Thesis, p 270, Department of Biochemistry and Molecular Biology, The University of Chicago, Chicago, IL.
46. Morais Cabral, J. H., Lee, A., Cohen, S. L., Chait, B. T., Li, M., and Mackinnon, R. (1998) Crystal structure and functional analysis of the HERG potassium channel N terminus: a eukaryotic PAS domain, *Cell 95*, 649−655.
47. Card, P. B., Erbel, P. J., and Gardner, K. H. (2005) Structural basis of ARNT PAS-B dimerization: use of a common beta-sheet interface for hetero- and homodimerization, *J. Mol. Biol. 353*, 664−677.
48. Yang, J., Zhang, L., Erbel, P. J., Gardner, K. H., Ding, K., Garcia, J. A., and Bruick, R. K. (2005) Functions of the Per/ARNT/Sim domains of the hypoxia-inducible factor, *J. Biol. Chem. 280*, 36047−36054.
49. Lario, P. I., Sampson, N., and Vrielink, A. (2003) Sub-atomic resolution crystal structure of cholesterol oxidase: what atomic resolution crystallography reveals about enzyme mechanism and the role of the FAD cofactor in redox activity, *J. Mol. Biol. 326*, 1635−1650.
50. Kemal, C., and Bruice, T. C. (1976) Simple synthesis of a 4a-hydroperoxy adduct of a 1,5-dihydroflavine: preliminary studies of a model for bacterial luciferase, *Proc. Natl. Acad. Sci. U.S.A. 73*, 995−999.
51. Palfey, B. A., and Massey, V. (1998) Flavin-dependent enzymes, in radical reactions and oxidation/reduction, in *Comprehensive Biological Catalysis*, pp 83−153, Academic Press, San Diego, CA.
52. Hummer, G., Schotte, F., and Anfinrud, P. A. (2004) Unveiling functional protein motions with picosecond x-ray crystallography and molecular dynamics simulations, *Proc. Natl. Acad. Sci. U.S.A. 101*, 15330−15334.
53. Key, J. (2004) Ph.D. Thesis, p 186, Department of Biochemisry and Molecular Biology, The University of Chicago, Chicago, IL.
54. Kort, R., Komori, H., Adachi, S., Miki, K., and Eker, A. (2004) DNA apophotolyase from *Anacystis nidulans*: 1.8 Å structure, 8-HDF reconstitution and X-ray-induced FAD reduction, *Acta Crystallogr., Sect. D: Biol. Crystallogr. 60*, 1205−1213.
55. Key, J., and Moffat, K. (2005) Crystal structures of deoxy and CO-bound bjFixLH reveal details of ligand recognition and signaling, *Biochemistry 44*, 4627−4635.
56. Erbel, P. J., Card, P. B., Karakuzu, O., Bruick, R. K., and Gardner, K. H. (2003) Structural basis for PAS domain heterodimerization in the basic helix−loop−helix-PAS transcription factor hypoxia-inducible factor, *Proc. Natl. Acad. Sci. U.S.A. 100*, 15504−15509.
57. Anderson, S., Dragnea, V., Masuda, S., Ybe, J., Moffat, K., and Bauer, C. (2005) Structure of a novel photoreceptor, the BLUF domain of AppA from *Rhodobacter sphaeroides*, *Biochemistry 44*, 7998−8005.
58. Gomelsky, M., and Klug, G. (2002) BLUF: a novel FAD-binding domain involved in sensory transduction in microorganisms, *Trends Biochem. Sci. 27*, 497−500.
59. Gauden, M., van Stokkum, I. H., Key, J. M., Luhrs, D., van Grondelle, R., Hegemann, P., and Kennis, J. T. (2006) Hydrogen-bond switching through a radical pair mechanism in a

flavin-binding photoreceptor, *Proc. Natl. Acad. Sci. U.S.A. 103*, 10895−10900.
60. Unno, M., Sano, R., Masuda, S., Ono, T. A., and Yamauchi, S. (2005) Light-induced structural changes in the active site of the BLUF domain in AppA by Raman spectroscopy, *J. Phys. Chem. B 109*, 12620−12626.
61. Little, R., Martinez-Argudo, I., and Dixon, R. (2006) Role of the central region of NifL in conformational switches that regulate nitrogen fixation, *Biochem. Soc. Trans. 34*, 162−164.
62. Money, T., Barrett, J., Dixon, R., and Austin, S. (2001) Protein-protein interactions in the complex between the enhancer binding protein NIFA and the sensor NIFL from *Azotobacter vinelandii*, *J. Bacteriol. 183*, 1359−1368.
63. Harper, S. M., Christie, J. M., and Gardner, K. H. (2004) Disruption of the LOV-Jalpha helix interaction activates phototropin kinase activity, *Biochemistry 43*, 16184−16192.

BI0620407